Indian Journal of Pure & Applied Physics
Vol. 60, January 2022, pp. 49-58

Investigations of absorption and magnetic resonance spectroscopies, molecular docking studies and quantum chemical calculations of 3-Hydroxy-4-methoxybenzaldehyde

K Parimala* & S Manimegalai

PG & Research Department of Physics, Nehru Memorial College (Affiliated to Bharathidasan University), Trichy-621 007, India

Received 27 September 2021; accepted 22 November 2021

The 3-Hydroxy-4-methoxybenzaldehyde (3H4MB) chemical has been explored experimentally and significantly using density functional theory (DFT) on the B3LYP/6- 311++G(d,p) technique as one of the derivatives of isovanillin, a phenolic aldehyde an organic substance. 3H4MB UV-Visible (800-100 nm), 1H NMR, and 13C NMR experiments have all been documented. The chemical shift measured by NMR is evaluated and compared to experimental values. Theoretical UV values were calculated using the TD-DFT approach and compared to experimental spectrum data, as well as oscillator strength and electron excitation energies. Charge transfer happens inside the molecule, according to the estimated HOMO–LUMO band gap energies. Chemical characteristics such as ionisation potential (I), electron affinity (A), hardness (η), and softness (σ) have been computed, as well as the molecule's chemical reactivity. The charge transfer and resonance of electron density within the molecule were studied using NBO analysis of the analyzed chemical. The molecular electrostatic potential (MEP) was investigated, and the resulting 3D image, which depicts the electrophilic and nucleophilic regions within the compound, was also drawn. We discovered that the molecule (3H4MB) had the lowest binding energy, which is –5.7, based on docking investigations.

Keywords: UV; B3LYP; NMR; DFT; HOMO-LUMO

1 Introduction

3-Hydroxy-4-methoxybenzaldehyde (3H4MB) is an intriguing chemical because of its simple phenolic structure, which consists of two hydroxyl (donor) groups and a carbonyl (acceptor) group on a benzene ring. In general, the presence of methoxy (OCH3) in a chemical group causes nonlinearity, resulting in the formation of a noncentrosymmetric crystal structure.

Antispasmodic action is found in plant-derived phenolic compounds such as benzaldehyde and benzyl alcohol, and some of them, such as piperonal or vanillin, have it to a greater extent and might be considered excellent candidates[1]. Isovanillin, a phenolic aldehyde found in many plants[2–5], inhibits aldehyde oxidase and is converted to isovanillic acid by aldehyde dehydrogenase[6, 7]. There is no official investigation on the pharmacological impact of isovanillin on gastrointestinal function, despite multiple studies on the vanillin isomer.

Acetovanillon (apocinin) is a naturally occurring organic compound that is structurally similar to vanillin. It was extracted from a variety of plant sources, and its far-reaching pharmacological properties are being studied. The anti-edema and anti-heart-problem capabilities of the vanillin molecule are used[8]. This study looked at the structure, UV and NMR spectra analysis, NBO, Fukui function, and thermal properties of the chosen molecule, as well as the findings. Frontier molecular orbitals analysis has also been used to explain information about the molecule's interactions with other species, which characterise the molecule's chemical reactivity. A molecular electrostatic potential (MEP) investigation was used to measure the chemical activity. As a result of its biological effect, molecular docking investigations have also been published. The fukui function is used to determine the local-softness and electrophilicity indices. However, no equivalent research has been done on 3H4MB to far.

2 Experimental Details

The 3-Hydroxy-4-methoxybenzealdehyde (3H4MB) molecule is available in solid form from Lancaster Chemical Company, with a purity claim of 97 percent. It was not further refined. Using Dimethyl sulfoxide (DMSO) as a solvent, a UV-Visible spectrophoto-

*Corresponding author: (E-mail: kparimala79@yahoo.co.in)

meter was used to get the molecule's UV-Vis spectrum in the wavelength range of 100–800 nm. The 13C (100 MHz: CDCl3) and 1H (400 MHz: CDCl3) nuclear magnetic resonance (NMR) spectra were recorded using a Bruker HC 400 instrument. The change in the chemical composition of protons in tetramethylsilane is depicted in parts per million (scale) (TMS).

3 Computational Details

The calculations were carried out with DFT of the three-parameter hybrid functional (B3)[9, 10] for the exchange portion and the Lee-Yang-Parr (LYP)[11] correlation function levels with the 6-311++G(d,p) basis set for the correlation function levels using the Gaussian 09W software[12]. The optimum structure, MEP surface, and Frontier molecular orbital studies of the present crystal were displayed using GaussView[13]. The GIAO technique was utilised to compute the 13C and 1H NMR isotropic shielding using the optimised parameters derived from the B3LYP/6-31++G(d,p) level of theory. The influence of solvent on theoretical NMR parameters was investigated using the PCM model. Using the isotropic shielding constant values, the isotropic chemical shifts (in ppm) for tetramethylsilane were computed (TMS). The Fukui function in the ground state was computed using the Mulliken population. Bonding molecular orbitals, lone pair molecular orbitals, and antibonding molecular orbitals were all handled by the NBO. The measured UV spectrum was compared to anticipated values using the Time dependent-DFT approach with liquid (water) phase to better understand the electrical properties. Molecular docking investigations were carried out using the Auto Dock Tool. The goal of this research was to show how (ligand-protein) binding occurs.

4 Result and Discussion

4.1. Structural analysis

The chemical structure of the 3H4MB is symmetrical in the C1 point group. Fig. 1 depicts the title molecule's optimized molecular structure. A benzene ring is linked to a hydroxyl, aldehyde and methoxy group in the chosen molecule.

4.2. Electronic experiments employing the TD-DFT approach

The B3LYP/6-311++G(d,p) level of theory and the time-dependent density functional theory technique were used to predict the calculated data for the title chemical 3H4MB. The spectrum that resulted was caught within the range and shown in Fig. 2. The estimated wavelength, excitation energy, and oscillation intensity are compared to the experimental results. According to this study, electronic absorption is the transition from an excited state to a ground state.

The calculated maximum absorbance of the title chemical was 221 nm, which matches the observed value of 211.83 nm in the UV-Visible spectrum. The transition from HOMO to LUMO causes absorption maxima in the spectrum, but the recorded range is wide enough to allow for further adjustments. To better understand the behaviour of electronic transitions, experimental and theoretical absorption maxima, oscillator field strength (f), energy, and significant contribution percentages of HOMO and LUMO for electronic transitions were compiled and

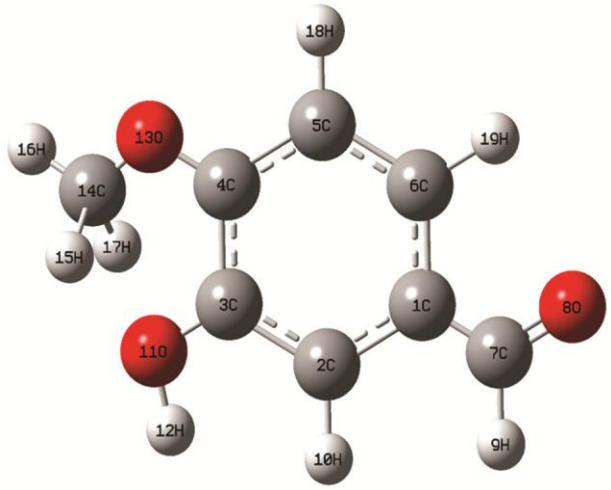

Fig. 1 — Optimized Molecular structure of 3H4MB along with numbering of atoms.

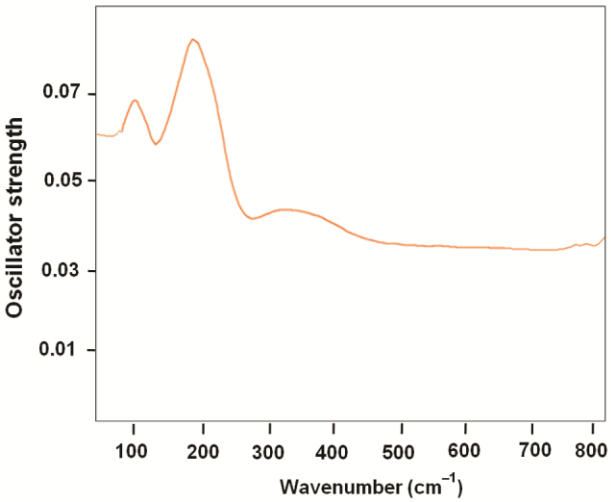

Fig. 2 — The experimental UV-Vis spectrum of 3H4MB.

summarized in Table 1. E = hc/λ is used to calculate the band gap energy. Here, hc is constant, and λ is cutoff wavelength equals. The band gap is the energy difference between HOMO and LUMO, and it is critical for structural stability[14]. The electric excitation from HOMO-LUMO contributes the most (88%) to the total contribution.

4.3. Molecular orbitals studies related to global descriptors

Because HOMO refers for highest occupied molecular orbital and LUMO means for lowest unoccupied molecule orbital, these are also known as boundary molecular orbitals. The HOMO and LUMO gaps reveal a lot about the chemical stability and reactivity of the molecule. According to Koopmans, HOMO and LUMO values in eV can predict Ionization potential (I), Electron affinity (A), HOMO-LUMO gap, hardness (η), Softness (σ), Chemical potential (μ), Electronegativity (χ), Electrofilicity index (ω), Total energy change (E_T), and Dipole moment (D). The molecule will be more polarizable and reactive if the energy difference between the molecules is small[15]. The HOMO, LUMO, and a few other key molecular orbitals, as well as their energies, were graphically depicted in Fig. 3. In Fig. 3, the red and green colours represent positive and negative signals, respectively. The HOMO covers the benzene ring, aldehyde and hydroxl groups in the molecule except for the methoxy group. The LUMO has spread the entire aldehyde group across the molecule except for the methoxy and hydroxyl groups. The parameters or chemical descriptors are listed in Table 2 along with their values. Using the formulas below, the HOMO and LUMO values were predicted to be –5.5985 eV and –0.8793 eV, respectively from the Table.

$$\Delta E = E_{LUMO} - E_{HOMO} \quad \text{... (1)}$$

$$\chi = \frac{-(E_{HUMO} + E_{LUMO})}{2} \quad \text{... (2)}$$

$$\eta = \frac{E_{LUMO} - E_{HUMO}}{2} \quad \text{... (3)}$$

$$\sigma = \frac{1}{\eta} \quad \text{... (4)}$$

$$\pi = -\chi \quad \text{... (5)}$$

$$S = \frac{1}{2\eta} \quad \text{... (6)}$$

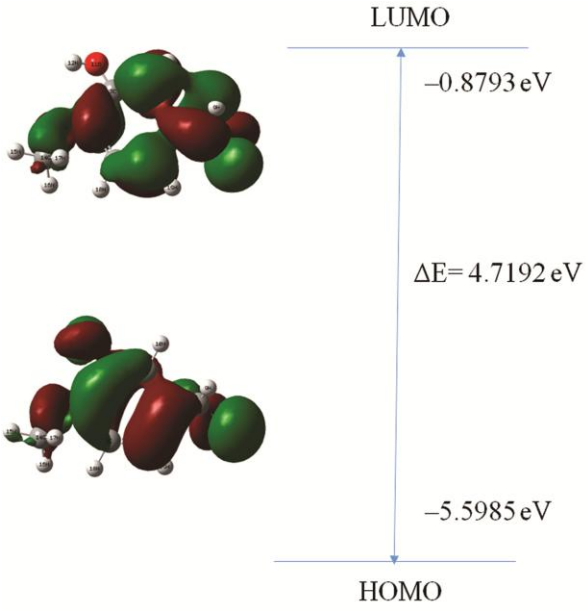

Fig. 3 — The atomic orbital components of the frontier molecular orbital (HOMO-MO: 40, LUMO-MO: 41) of 3H4MB.

Table 2 — The energies of frontier molecular orbitals and global reactivity descriptors of 3H4MB.

Property	Energies (eV)
Total energy (eV)	–18042.86
E_{HOMO} (eV)	–5.5985
E_{LUMO} (eV)	–0.8793
E_{HOMO}–E_{LUMO} (eV)	4.7192
Ionization potential (I) (eV)	5.6778
Electron Affinity (A) (eV)	0.8467
Chemical potential (μ) (eV)	–4.2069
Electronegativity (χ) eV	3.5629
Chemical hardness (η)eV	–3.4857
Electrofilicity index (ω) eV	2.4724
Global Softness (σ) eV	0.4812
Total energy change (ΔE_T) eV	–0.6314
Dipole moment (D)	5.2495

Table 1 — The experimental (Exp.) and calculated (Cal.) absorption wavelength λ (nm), excitation energies E (eV) and oscillator strengths (*f*) of 3H4MB calculated by TD-DFT/B3LYP/6-311++G(d,p) level of theory in water solvent phase.

Wavelength λ (nm)		Band gap (ev)	oscillator strengths (*f*)	Energy (cm^{-1})	Type	Assignment
Exp.	Cal.					
	389.02	6.3235	0.009	36523.52	n→π*	HOMO→LUMO (88%)
	315.42	6.3235	0.018	52861.23	π→π*	H–2→LUMO (14%), HOMO→L+1 (83%)
	279.81	6.7143	0.006	43392.34	π→π*	H–3→LUMO (85%)
	276.14	6.8545	0.004	45493.38	π→π*	H–1→LUMO (74%), H–2→L+1 (11%), HOMO→L+1 (9%), HOMO→L+2 (7%)
221	211.83	5.9813	0.007	46774.54	π→π*	H–2→LUMO (59%), H–1→L+1 (33%), H–2→L+1 (6%), HOMO→L+1 (14%)

$$\omega = \frac{\pi^2}{2\eta} \quad \text{... (7)}$$

The energy gap was 4.7192 eV which represents the electrical conductivity of the investigated molecule. From the basis of Koopman's theorem, the computed values of the titled compound were, Ionization potential (I) = 5.6778 eV, Electron Affinity (A) = 0.8467 eV, Chemical potential (μ) = –4.2069 eV, Electronegativity (χ)= 3.5629 eV, Chemical hardness (η) = –3.4857 eV, Electrofilicity index (ω)= 2.4724 eV, Global Softness (σ) = 0.4812 eV, Total energy change (ΔE_T) = –0.6314, Dipole moment (D) =5.2495 Debye.

4.4. Molecular electrostatic potential (MEP) maps

To investigate the charge distribution, molecular reactive behavior, nucleophilic and electrophilic nature V(r) of molecules MEP is an important tool. It is through this potential V(r) is given by

$$V(\vec{r}) = \sum_A \frac{Z_A}{|\vec{R} - \vec{r}|} - \int \frac{\rho(\vec{r}')dr'}{|\vec{r}' - \vec{r}|} \quad \text{... (8)}$$

where Z_A is the charge on nucleus A, which is located at R_A, and ρ(r') is the molecule's electronic density function[16, 17]. The electrostatic potential is denoted by several colors; blue denotes a positive electrostatic potential, red denotes a maximum negative electrostatic potential, yellow denotes a slight negative electrostatic potential, and green denotes a zero potential region[18, 19]. Red and blue colors were used to indicate the electrophilic and nucleophilic portions of the molecule, respectively. Green was used to indicate neutral electrostatic potential. Green color represents the zone with no electrostatic potential. The electrophilic and nucleophilic areas of the molecule's surface are highlighted in red and blue, respectively. Fig. 4 depicted the three-dimensional depiction of the named molecule. In general, the negative charge that can be targeted by electrophile is represented by the red region. Similarly, the blue zone represents the highest positive charge that a nucleophile can attack. Aldehyde group oxygen atom in this molecule are electrophiles, which means they are in the red area. In the blue area, the hydroxyl group hydrogen atom act as nucleophiles.

4.5. NBO analysis

The molecular structure of the designated chemical 3H4MB was investigated via NBO analysis. Donors, bonding, lone pair orbitals, empty orbitals (donors), and anti-bonding orbitals are all revealed by the NBO analysis of filled orbitals. The NBO study's purpose was to learn more about the donor-acceptor relationship. The lack of occupancy from the Lewis design's localized NBO to the non-Lewis orbital causes these interactions. Calculate the stabilization energy using the donor (i) and acceptor (j) as inputs, with i and j's conjugation expected to be as follows:

$$E^{(2)} = -n_\sigma \frac{\langle \sigma|F|\sigma\rangle^2}{\varepsilon_{\sigma^*} - \varepsilon_\sigma} = -n_\sigma \frac{F_{ij}^2}{\Delta E} \quad \text{... (9)}$$

Here $\langle \sigma|F|\sigma\rangle^2$ or F_{ij}^2 is the Fock matrix component i and j NBO orbital, ε_{σ^*} and ε_σ are the energies of σ and σ* NBO's and n_σ is the population of the contributor σ orbital and $E^{(2)}$ stabilization energy.

The higher the $E^{(2)}$ reflects the stabilizing energy, the more delocalization inside the molecule. Table 3 shows the computed stabilization energy $E^{(2)}$ between donor and acceptor orbitals. Table 3 shows that the interactions between π of C1–C6, C2–C3, C4–C5 to anti-bonding orbitals π* of C7–H9, C1–C6, and C1–C2 have delocalization energies of 244.16 kJ/mol, 161.22 kJ/mol, and 149.17 kJ/mol, respectively, which constitute the highest delocalization and inter charge transfer within the molecule. These highest energy values also imply that the bond's weakness is due to a lot of delocalization within the molecule. The lone pair of O11, O13 to the anti-bonding π* of C3–C4, C14–H15 in the benzene ring had moderate delocalization energies of 80.67 kJ/mol and 53.33 kJ/mol, respectively, indicating important interactions in the studied molecule. The stabilizing energy of the (O13–C14) interaction with σ* of C3–C4, C4–C5, and C4–O13 is 99.79 kJ/mol, 95.75 kJ/mol, and 87.92 kJ/mol, respectively. The interaction energy

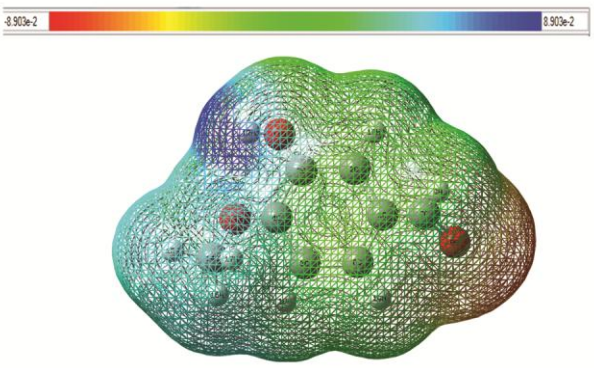

Fig. 4 — The Molecular Electrostatic potential (MEP) for the 3H4MB compound.

Table 3 — The donor-acceptor interactions and their stabilization energies of 3H4MB on NBO basis.

Donor (i)	Type	Ed/e	Acceptor (j)	Type	Ed/e	[a]E(2) KJ/mol	[b]E(i)-E(j) (a.u)	[c]F(i,j) (a.u)
C1–C2	σ	1.9769	C1–C6	σ*	0.0291	5.73	1.24	0.075
			C1–C7	σ*	0.0236	15.05	1.78	0.147
			C7–H9	σ*	0.8457	4.78	1.05	0.063
C1–C6	π	1.9234	C2–C3	π*	0.2365	16.08	0.26	0.060
			C4–C5	π*	0.5894	17.24	0.25	0.059
			C7–O8	π*	0.2378	83.40	0.26	0.133
			C7–H9	π*	0.2598	1.85	0.63	0.034
C1–C7	σ	1.9832	C1–C2	σ*	0.9874	10.70	1.50	0.114
			C1–C6	σ*	0.1289	12.63	1.50	0.123
			C7-H9	σ*	0.5871	3.19	1.31	0.058
C2–C3	σ	1.9421	C1-C2	σ*	0.6912	2.82	1.28	0.054
C2–C3	π	1.9256	C1–C6	π*	0.3913	19.41	0.31	0.072
			C7–O8	π*	0.2654	1.11	0.28	0.016
C2–H10	σ	1.9263	C1–C2	σ*	0.5672	1.03	1.10	0.030
			C3–O11	σ*	0.3652	1.32	1.32	0.037
			O11–H12	σ*	0.4236	1.10	0.85	0.027
C3–C4	σ	1.9783	C2–C3	σ*	0.2654	4.29	1.27	0.066
			C2–H10	σ*	0.3678	1.76	1.14	0.040
			O11–H12	σ*	0.6451	5.46	1.05	0.068
			O13–C14	σ*	0.9514	6.43	0.93	0.069
C3–O11	σ	1.9653	C2–C3	σ*	0.8412	3.87	1.89	0.077
			O11–H12	σ*	0.1297	0.92	1.66	0.035
C4–C5	σ	1.9836	C3–C4	σ*	0.6325	4.19	1.24	0.065
C4–C5	π	1.9287	C1–C6	π*	0.5647	21.16	0.32	0.075
			C2–C3	π*	0.2354	16.27	0.30	0.063
			C14–H15	π*	0.5874	0.68	0.66	0.021
C4–O13	σ	1.9854	C2–C3	σ*	0.6987	0.86	1.86	0.036
			O13–C14	σ*	0.2365	1.73	1.52	0.046
C5–C6	σ	1.9632	C1–C6	σ*	0.5897	2.26	1.28	0.048
			C4–O13	σ*	0.2565	2.67	1.51	0.057
			C6–H19	σ*	0.3654	0.82	1.12	0.027
C5–H18	σ	1.9498	C1–C6	σ*	0.9871	3.06	1.11	0.052
			C3–C4	σ*	0.5641	3.54	1.06	0.056
			C4–O13	σ*	0.4562	1.22	1.34	0.036
			C5–C6	σ*	0.2315	0.89	1.11	0.028
C6–H19	σ	1.9236	C1–C2	σ*	1.3654	4.40	1.11	0.063
			C4–C5	σ*	1.3254	3.61	1.07	0.056
			C5–C6	σ*	0.8742	0.59	1.10	0.023
C7–O8	σ	1.9745	C1–C6	σ*	0.5468	10.90	1.41	0.111
			C1–C7	σ*	0.2987	6.05	1.95	0.097
C7–O8	π	1.9832	C1–C6	σ*	0.2687	2.39	0.91	0.042
			C1–C6	π*	0.5943	23.25	0.38	0.093
C7–H9	σ	1.9236	C1–C2	σ*	0.6587	12.35	1.07	0.103
			C1–C6	σ*	0.3215	0.76	1.06	0.025
			C7–O8	π*	0.1256	0.51	0.50	0.016
O11–H12	σ	1.9489	C2–C3	σ*	0.5648	93.81	1.34	0.044
			C3–C4	σ*	0.2365	12.34	1.31	0.115
			C3–O11	σ*	0.5987	0.74	1.59	0.031
O13–C14	σ	1.9412	C3–C4	σ*	0.2987	99.79	1.38	0.073
			C4–C5	σ*	0.1235	95.75	0.85	0.070
			C4–O13	σ*	0.0654	87.92	1.65	0.050
C14–H15	σ	1.9856	C4–O13	σ*	0.2654	2.90	1.39	0.046
C14–H16	σ	1.9294	C4–O13	σ*	0.3612	8.87	1.39	0.031
C14–H17	σ	1.9854	C4–O13	σ*	0.9541	9.67	1.39	0.027
			O13–C14	σ*	0.5231	0.78	0.80	0.023
O8	LP	1.9321	C1–C2	σ*	0.4236	0.96	1.27	0.031
			C1–C7	σ*	0.1269	0.52	1.80	0.027
			C7–H9	π*	0.2654	10.48	0.62	0.072

(*Contd*.)

Table 3 — The donor-acceptor interactions and their stabilization energies of 3H4MB on NBO basis (*Contd*.).

Donor (i)	Type	Ed/e	Acceptor (j)	Type	Ed/e	[a]E(2) KJ/mol	[b]E(i)-E(j) (a.u)	[c]F(i,j) (a.u)
O11	LP	1.9654	C2–C3	σ*	0.3987	9.77	1.16	0.095
			C3–C4	σ*	0.2547	3.49	1.12	0.056
			C3–C4	π*	0.5689	80.67	0.40	0.165
O13	LP	1.9238	C3–C4	σ*	0.2147	8.58	1.04	0.079
			C14–H15	π*	0.8945	53.33	0.89	0.049
O13	LP	1.9583	C3–C4	π*	0.2365	5.77	0.93	0.068
			C4–C5	σ*	0.2145	3.11	0.95	0.051
			C14–H17	σ*	0.9871	3.91	0.77	0.052
C1–C6	π	0.3652	C7–H9	π*	0.8974	244.16	0.35	0.061
C2–C3	π	0.6521	C1–C6	π*	0.2365	161.22	0.02	0.075
C4–C5	π	0.8923	C1–C2	π*	0.5478	149.17	0.03	0.077
			C2–C3	π*	0.2136	0.16	0.02	0.089
			O13–C14	π*	0.2365	4.23	0.21	0.056
C7–O8	π*	0.9845	C1–C2	σ*	0.8123	0.64	0.57	0.036
			C1–C6	π*	0.1259	39.00	0.02	0.124

[a]$E^{(2)}$ means energy of hyper conjugative interaction (stabilization energy).
[b]Energy difference between donor(i) and acceptor(j) NBO orbitals.
[c]F(i,j) is the fork matrix element between i and j NBO orbitals.

Table 4 — The experimental and calculated ^{13}C and ^{1}H NMR isotropic chemical shifts (δ in ppm) of 3H4MB by B3LYP/6-311++G(d,p) level of theory.

Atoms	δppm (Calculated)	Experimental	Atoms	δppm (Calculated)	Experimental
C1	82.08	80	H9	9.786	9.8
C2	114.65	115	H10	0.426	0.3
C3	118.09	118	H12	7.412	7.2
C4	127.62	127	H15	7.835	7.5
C5	145.75	134	H16	9.347	9.2
C6	152.06	150	H17	3.995	4.2
C7	153.48	156	H18	4.045	
C14	194.96	195	H19	4.125	

between the σ of (O11–H12) to the σ*of C2–C3 is 93.81 kJ/mol was another significant interaction within the molecule. From the results discussed above, we concluded that the interaction between π→π* was more probable than the remaining transitions, i.e., σ→π*, LP→π*.

4.6. NMR Spectral Analysis

Table 4 lists the 1H and 13C NMR chemical shift values calculated at the B3LYP technique with 6-311++G(d,p) basis set and chloroform solvent, as compared to their observed values in CDCl3 solvent for TMS as an internal reference[20], as detailed in the computational details section. Table 4 demonstrates that the title compound exhibits greater 13C chemical shift values for carbon atoms linked to oxygen atoms in the aromatic ring and the aldehyde group, which are C14 and C7, respectively, in both the aromatic ring and the aldehyde group. Due to the electronegative feature of the oxygen atom, the chemical shift values of the specified carbon atoms become bigger than the others, and the calculated/observed values are as follows: 194.96/195 ppm for the C14 atom and 153.48/156 ppm for the C7 atom. Furthermore, as indicated in Table 4, the H9 atom, which belongs to the aldehyde group, has a greater 1H NMR chemical shift value, with an experimental/calculated value of 9.8/9.786 ppm. Table 4 shows how well the title molecule's anticipated 13C and 1H NMR chemical shift values match the actual data in Fig. 5.

4.7. Reactive descriptors

The condensed Fukui functions (f_k) were estimated using Yang and Mortier's[21] simple approach (based on Mulliken population analysis). Independent computations for matching N+1, N1 and N are total electrons present in anion, cation, and neutral states of molecules, respectively, are required for a system of N electrons. For all atoms, Muilliken population analysis produces (gross charges) $q_k(N+1)$, $q_k(N–1)$, and $q_k(N)$. The condensed Fukui functions were given by the equations in a restricted distinction estimation:

for nucleophilic attack $f_k^+ = q_k(N+1) - q_k(N)$ ... (10)

for electrophilic attack $f_k^- = q_k(N) - q_k(N-1)$ ... (11)

for free radical attack $f_k^0 = \frac{1}{2}[q_k(N+1) - q_k(N-1)]$ ... (12)

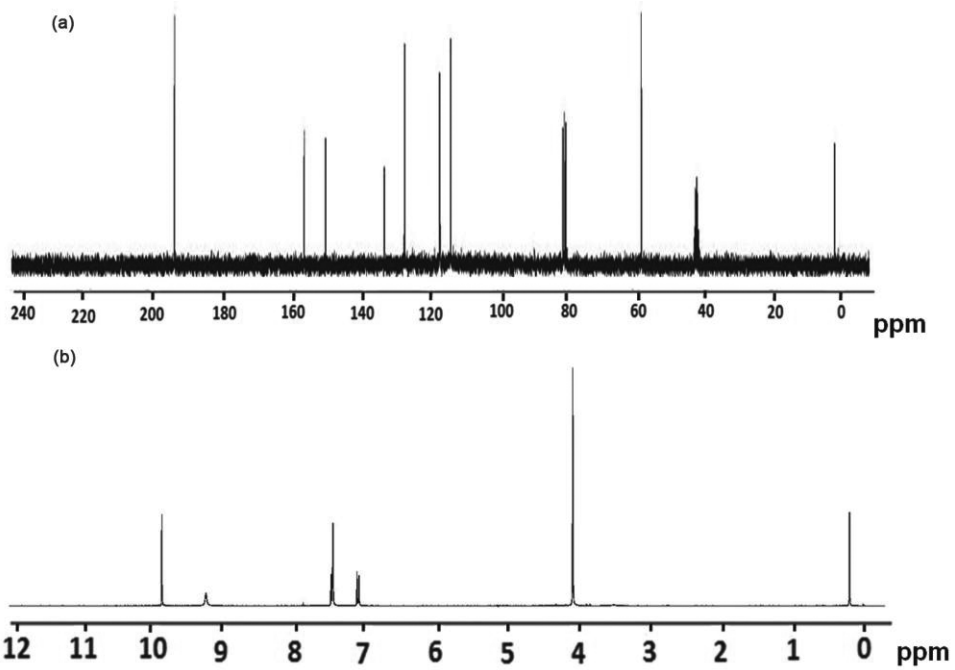

Fig. 5 — The experimental (a) ^{13}C and (b) ^{1}H NMR spectra of 3H4MB.

The condensed-to-atom quantity, ω_k^α corresponding to local elecrophilisity index, $\omega(r)$, was obtained as described previously[22]:

$$\omega_k^\alpha = \omega f_k^\alpha \quad \text{... (13)}$$

where α = +, –, and 0 refer to nucleophilic, electrophilic and free radical reactions, respectively.

Chemical selectivity in a chemical system at a single place is described using local reactivity descriptors, such as Fukui functions[23]. The fukui function is defined as the sum of the electron density, the number of electrons, and the nucleus' external potential[24]. Several groups have attempted to tackle the problem of the negative Fukui function[25]. The lower value represents the site of an electrophilic attack order, according to Table 5 of 3H4MB: C14>O8>O11>H12>C5>C7>C2. The nucleophilic site order predicted by the computed values is C1>C4>H18>H9>H15>C3.

O13>C6>H16>H17>H10>H19 was the attack for free radicals. It is clear that the reactivity of the atoms that are more stable than the others decreases.

Table 5 — Fukui indices for nucleophilic and electrophilic and free radical sites on 3H4MB atoms computed Mulliken charges according with equation (10–13) at B3LYP method with 6-311++G(d.p) basis set.

Atoms	f_k^+	f_k^-	f_k^0
C1	0.583	0.213	–0.017
C2	–0.225	–0.243	–0.118
C3	0.299	0.225	–0.092
C4	0.425	0.025	–0.225
C5	–0.376	–0.326	–0.027
C6	–0.104	0.077	0.439
C7	–0.065	–0.321	–0.221
O8	–0.007	–0.456	–0.275
H9	0.408	0.006	–0.224
H10	–0.045	0.457	0.326
O11	–0.125	–0.446	–0.166
H12	–0.032	–0.339	–0.045
O13	–0.814	0.037	0.449
C14	–0.453	–0.459	–0.007
H15	0.304	0.246	–0.164
H16	–0.025	0.084	0.435
H17	–0.016	0.037	0.427
H18	0.412	0.459	–0.623
H19	–0.056	0.264	0.072

4.8. Thermo molecular characteristics

Some thermo molecular characteristics, such as zero-point vibrational energy, enthalpy, Gibbs free energy, internal energy, entropy, heat capacity, thermal energy, and partition functions (Fig. 6) have been found to be critical in material characterization and understanding of reactivity or mode of action, as well as environmental influences on the mole. The examination of the thermodynamic properties of the title chemical chosen for this investigation is highly fascinating. The heat capacity (Cp), enthalpy changes (H–E/T), entropy (S), and Gibbs free energy (G–E/T) statically thermodynamic functions for the title molecule were determined from theoretical

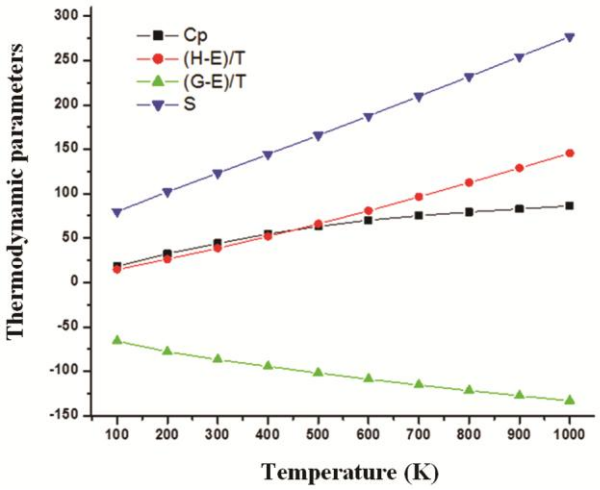

Fig .6 — Correlation graph of heat capacity, entropy, enthalpy and Gibb's free energy with temperature for 3H4MB.

Table 6 — Thermodynamic properties of 3H4MB at different temperatures calculated by B3LYP/6-311++G(d,p) method.

Temp (K)	Cp (calmol^{-1}K^{-1})	(H-E)/ T (kcalmol^{-1})	S (kcalmol^{-1})	(G-E)/ T (kcalmol^{-1})
100	18.634	14.919	79.943	–65.937
200	32.437	26.434	102.235	–77.896
300	44.223	38.587	123.117	–86.638
400	54.718	51.916	144.315	–94.415
500	63.274	66.133	165.896	–101.874
600	69.998	80.965	187.774	–108.817
700	75.293	96.584	209.862	–115.394
800	79.498	112.573	231.992	–121.635
900	82.904	128.957	254.395	–127.454
1000	86.436	145.668	276.757	–133.203

thermodynamic parameters via vibration analysis. The thermodynamic values are useful for further research on the title compounds, particularly when used as a reactant in a novel method. Several thermodynamical features are listed in Table 6 of 3H4MB that can be utilized to predict chemical reactivity and stability of compounds. As the temperature rises, all of the investigated thermodynamic parameters increase, while (G–E/T) decreases (Fig. 6). The molecule's enthalpy (H–E/T) and entropy (S) variations suggested that it is more adaptive to changing its thermodynamic system for temperature. All of the fitting parameters, as well as other relevant statistical variables and their fitted graphs, have been displayed. The fitting equations for the thermal characteristics of 3H4MB are as follows:

$$Cp=3.435+0.312T-0.009T^{2}\left(R^{2}=0.999\right) \quad \ldots (14)$$

$$\left(H-E\right)/T=0.587+0.265T-0.005T^{2}\left(R^{2}=0.999\right) \quad \ldots (15)$$

$$\left(G-E\right)/T=-66.69-0.138T-0.009T^{2}\left(R^{2}=0.999\right) \quad \ldots (16)$$

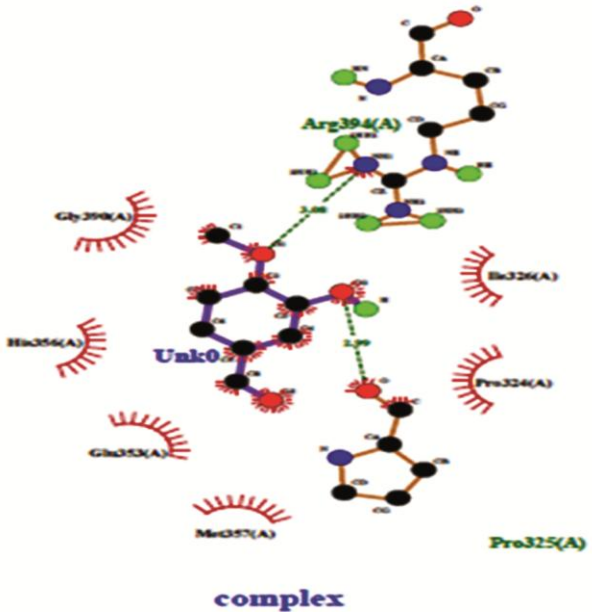

Fig. 7 — 2-D interaction plot of the ligand at the active site of the protein showing *pi-pi* stacking and hydrogen bond for 3H

$$S=59.18+0.294T-0.007T^{2}\left(R^{2}=1.000\right) \quad \ldots (17)$$

The proper fitting equations, as well as the correlation graphs from Fig. 6, are shown here. All of the thermodynamic data on the 3H4MB is important for future research. All thermodynamic calculations were performed in the gas phase and were not applicable to the solution. All of the thermal molecular data is crucial for future research on the title molecule. The thermodynamic parameters can be used to compute other thermodynamic features using thermodynamical estimation of parameters and directions of chemical processes according to the second law of thermodynamics in the subject of thermochemistry.

4.9. Molecular Docking

Using in silico molecular docking on 3H4MB analogues, the best-matched molecules and molecular binding interactions were found. The human Estrogen Receptor Ligand-Binding Domain (hERLBD) in combination with 4-hydroxytamoxifen (PDB: 3ERT) was retrieved from the Protein Data Bank and modified before being used in a molecular docking investigation to determine the compound's binding interactions (3H4MB). The docking investigation was conducted out in extreme precision (XP) mode with the Schrödinger Glide software (Maestro 12.7)[26, 27]. The best scoring posture for the chemical (3H4MB) from the docking trials is shown in Figs. 7 and 8, along with

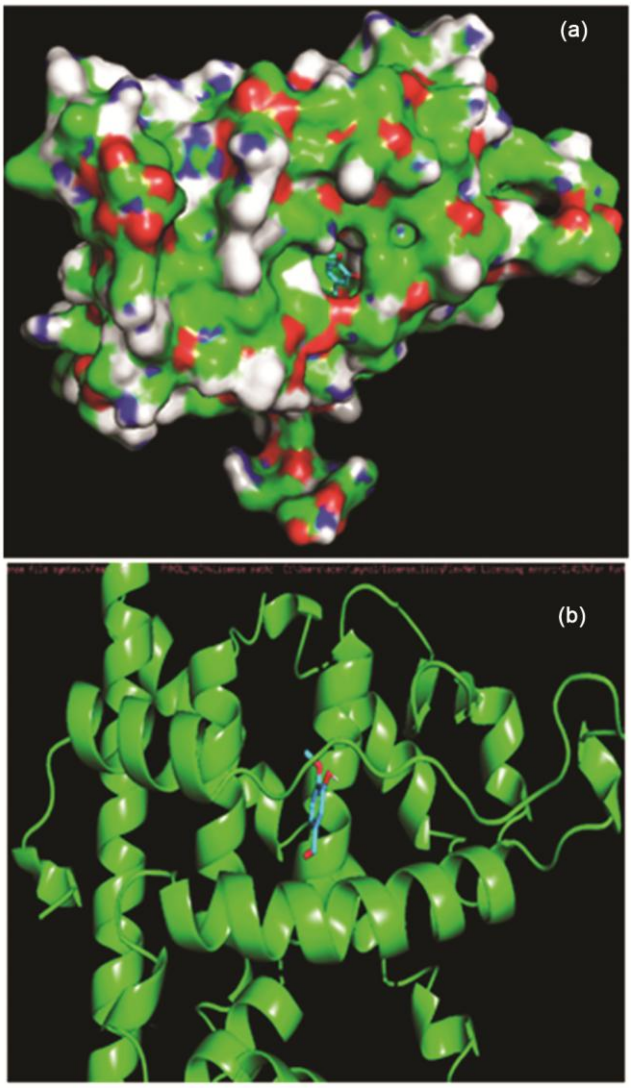

Fig. 8 — (a) 3-D visualisation of the ligand-protein complex with close view showing the enfolding of the ligand in the active site and (b) Ribbon model of the protein showing hydrogen bond with ligand as dashed lines to 3H4MB.

the important residues inside the binding site. Based on docking testing, we discovered that the molecule (3H4MB) has the lowest binding energy, which is –5.7. Through docking experiments, we showed that the majority of the ligands form hydrogen bonds with the residues (ASP 351, Water), as well as Van der Waals (VdW) interactions with the surrounding hydrophobic residues GLU 353, ARG 394, THR 347, MET 343, LEU 346, and LEU 349 inside the Helix[27]. Table 7 presents the ligand-ER (PDB: 3ERT) protein interaction with the lowest binding strength as determined via glide molecular docking.

Table 7 — Lowest binding energy for the ligand 3H4MB and ER protein (PDB: 3ERT).

Mode	Affinity (kcal/mol)	Dist from best mode	
		rmsd l.b.	rmsd u.b.
1.	–5.7	0.000	0.000
2.	–5.5	1.378	4.120
3.	–5.4	1.125	4.213
4.	–5.4	1.676	4.295
5.	–4.7	19.456	20.871
6.	–4.4	20.008	20.993
7.	–4.4	18.843	20.176
8.	–4.3	17.813	19.357
9.	–4.3	17.864	18.529

5 Conclusion

The ideal shape of 3H4MB was discovered using the B3LYP DFT approach with the 6-311++G(d,p) basis set. UV and NMR (13C and 1H) spectra comparisons of the expected bands are often in good agreement with experimental results. Future research on the title chemical will benefit from the thermodynamic data. The HOMO and LUMO energy gaps of the top compound (4.7192 eV) were calculated. Oxygen atoms are shown in negative potential sites on the MEP map, whereas hydrogen atoms are shown in positive potential sites; these sites reflect the region where the molecule might interact with other molecules and form metallic bonds. The acceptor-donor interactions energies, such as stabilization energy, charge transfer inside the molecule, and hyperconjugative stabilization, were calculated using NBO analysis. The electrophilic and nucleophilic regions of the identified molecule were determined using MEP analysis, and the relevant three-dimensional surfaces of the molecule were drawn. Fukui functions define the head line molecule's chemical activity and selectivity. Correlations between statistical thermodynamic data and temperature can also be found. A molecular docking study was used to predict the binding interactions of 3H4MB with the Estrogen Receptor (3ERT), and the results were evaluated.

References

1 Vidal J P, *Kirk-Othmer Encyclopedia of Chemical Technology*, Wiley Online Library, 2006.
2 Yang L, Feng F & Gao Y, *J Chin Mater Medica*, 34 (2009) 1805.
3 Xu J, Tan N, Zeng G, Han H, Huang H, Ji C, Zhu M & Zhang Y, *J Chin Mater Medica*, 34 (2009) 990.
4 Chen W, Tang S, Qin N, Zhai H & Duan H, *J Chin Mater Medica*, 37 (2012) 806.
5 Khaliq-uz-Zaman S M, Simin K & Ahmad V U, *Fitoterapia J*, 71 (2000) 331.

6 Lee K, Park S K, Kwon B M, Kim K, Yu H E, Ryn J, Oh S J, Lee K S, Kang J S, Lee CW, Kwon M G & Kim H M, *Xenobiotica J*, 29 (2009) 881.

7 Panoutsopoulos G I & Beedham C, *Pharmacol J*, 73 (2005) 199.

8 Dodd J M & Pearse D B, *Am J Physiol*, 279 (2000) 303.

9 Hohenberg P & Kohn W, *Phys Rev*, 136 (1964) 864.

10 Becke A D, *J Chem Phys*, 98 (1993) 5648.

11 Lee C, Yang W & Parr R G, *Phys Rev B*, 37 (1998) 785.

12 Frisch M J, *et al.*, Gaussion 09W Program, Gaussian, Inc, Wallingford, CT, 2004.

13 Gaussview, Roy D, Keith T & Millam J, Semichem Inc, Shawnee Mission, KS, (2009).

14 Lewis D F V, Loannides C & Parke D V, *Xenobiotica J*, 24 (1994) 401.

15 Renjith R, Sheena M Y, Tresa V H, Yohannan P C, Thiemann T, Shereef A & Al-Saadi A A, *J Phys Chem Solids*, 87 (2015) 110.

16 Drissi M, Chouaih A, Megrouss Y & Hamzaoui F, *J Crystallog*, 2013 (2013) 1.

17 Sirocco E & Tomasi J, *Adv Quantum Chem*, 11 (1978) 115.

18 Ignatov S K, Moltran V2.5 – Program for Molecular Visualization and Thermodynamic Calculations, University of Nizhny Novgorod, 2004.

19 Morris G M & Lim-Wilby M, Molecular docking, In Molecular modeling of proteins, *Humana Press*, chapter 19 (2008) 365.

20 National Institute of Advanced Industrial Science (2009), SDBS http://riodb01.ibase.aist.go.jp/sdbs.

21 Yang W & Mortier W J, *J Am Chem Soc*, 108 (1986) 5708.

22 Chattaraj P K, Maiti B & Sarkar U, *J Phys Chem A*, 107 (2003) 4973.

23 Yang W & Parr R G, *Proc Natl Acad Sci*, 82 (1985) 6723.

24 Parr Y R G, Functional Theory of Atoms and molecules, Oxford University press, New York, 1989.

25 Roy R K, Hirao H, Krishnamurthy S & Pal S, *J Chem Phys*, 115 (2001) 2901.

26 Schrödinger L L C, New York, N Y Glide, Ver. 6 (2013) 1.

27 Maruthanila V L, Elancheran R, Roy N K, Bhattacharya A, Kunnumakkara A B, Kabilan S & Kotoky J, *Curr Comput Aided Drug Des*, 15 (1) (2019) 89.